The following publication U. Karaagac, J. Mahseredjian, S. Jensen, R. Gagnon, M. Fecteau and I. Kocar, "Safe Operation of DFIG-Based Wind Parks in Series-Compensated Systems," in IEEE Transactions on Power Delivery, vol. 33, no. 2, pp. 709-718, April 2018 is available at https://doi.org/10.1109/TPWRD.2017.2689792.

Safe Operation of DFIG based Wind Parks in Series Compensated Systems

U. Karaagac, *IEEE Member*, J. Mahseredjian, *IEEE Fellow*, S. Jensen, R. Gagnon, M. Fecteau, *IEEE Member*, I, Kocar, *IEEE Senior Member*

***Abstract*— Subsynchronous control interaction (SSCI) is the interaction between the power electronics control and the series compensated transmission system that occurs at frequencies below the system nominal frequency. SSCI may occur between the doubly-fed induction generator (DFIG) control system and the series compensated transmission line, to which the wind park (WP) is connected. Not only the DFIG control system parameters, but also the WP operating conditions have significant impact on SSCI. In this paper the impact of WP operating conditions and DFIG control system parameters on SSCI are analyzed in details. Guidelines are presented for modifying the DFIG control system parameters to ensure safe operation and acceptable transient responses due to faults. This paper also examines the accuracies of various analytical tools used for SSCI problem identification and proposes a new frequency scan analysis approach for accurate prediction of potential SSCI problems.**

***Index Terms*— Doubly-fed induction generator (DFIG), eigenvalue analysis, electromagnetic transient (EMT) simulation, frequency scan analysis, series capacitor compensation, subsynchronous control interaction (SSCI), wind park.**

I. Introduction

Recent studies have identified the vulnerability of series compensated doubly-fed induction generator (DFIG) based wind parks (WPs) to subsynchronous interaction control (SSCI) [1],[2]. This was confirmed in October 2009 with the SSCI incident in the Zorillo Gulf WP in Texas [3]-[5]. There has recently been a growing interest in developing effective SSCI mitigation methods [6]-[12].

In [1]-[2], the impact of WP operating conditions and DFIG control system parameters on SSCI was analyzed using simple linearized models to identify the range of DFIG control system parameters for safe operation. However, these studies do not discuss the feasibility of the identified DFIG control system parameter range considering WT transient performance. It should be noted that, such a complementary study requires electromagnetic transient (EMT) simulations using detailed DFIG models that include the nonlinearities (in both electrical and control system model) and essential transient functions to fulfill the grid code requirement regarding fault-ride-though (FRT) [13]. The studies in [1]-[2] also disregard the DFIG input measuring filters although their impact on SSCI is significant.

U. Karaagac is with The Hong Kong Polytechnic University, Hong Kong; J. Mahseredjian and I. Kocar are with École Polytechnique de Montréal, Montréal, QC, Canada; S. Jensen is with Senvion SE, Hamburg, Germany; R. Gagnon is with IREQ, Varennes, QC, Canada; M. Fecteau is with Hydro-Québec TransÉnergie, Montréal, QC, Canada.

The SSCI mitigation methods based on supplementary control signal (or signals) usage in DFIG control [8]-[12] are quite promising due to their low investment costs. However, further research is required to conclude on the effectiveness and/or feasibility of these methods due to following reasons:

- The possible negative impact of the proposed SSCI damping controller on DFIG transient response during faults has been disregarded,
- The considered WP models have been obtained by scaling up a WT model to the desired power without taking the WP controller (WPC) into account, i.e. the reactive power control schemes are not realistic,
- No research has been reported on the implementation of an SSCI mitigation method in an actual WP.

It should be emphasized here that, the implementation of these mitigation methods in an actual WP brings several challenges due to possible communication requirement between the central SSCI controller and DFIGs such as variable communication network latency. Hence, it is desirable to mitigate the SSCI problem by modifying DFIG control system parameters while achieving acceptable transient performance.

This paper presents the impact of WP operating conditions, DFIG control system parameters and DFIG input measuring filters on SSCI, and finally proposes a guideline for tuning DFIG control system parameters that ensures safe operation and acceptable transient response to the faults. This paper also examines the accuracy of frequency scan and eigenvalue analysis results by comparing with the EMT simulations and investigates the sources of discrepancies. In addition, this paper proposes a new frequency scan analysis approach for accurate prediction of SSCI problem.

The first part of this paper briefly presents the WPs with DFIGs studied in this paper. The second part presents the system under study, demonstrates the impact of WP operating conditions and DFIG control system parameters on SSCI, and compares the eigenvalue analysis results with EMT simulations. The third part presents the proposed frequency scan analysis approach and examines the impact of DFIG input measuring filters on SSCI. The last part demonstrates SSCI mitigation with DFIG control system parameter modification

and presents a guideline for safe and acceptable operation.

II. Wind Parks with DFIG Wind Turbines

A simplified single line diagram of a typical wind park is shown in Fig. 1. In wind parks, WTs are connected through a step-up transformer (not shown in Fig. 1) to the medium voltage (MV) collector bus by means of subterranean cables. The collector bus voltage is stepped up to the HV level by means of wind park transformer. Although not shown in Fig. 1, the WP transformer has an on-load-tap-changer (OLTC) to keep the MV collector bus voltage at its nominal value.

The active power at the point of interconnection (POI in Fig. 1) depends on the wind conditions at each WT inside the WP and is determined by the maximum power point tracking (MPPT) function when the wind speed is between cut-in and rated speed. According to usual grid code requirements, the WP has a central wind park controller (WPC) to control the reactive power at the POI. The WPC can be actually set to control, either reactive power, voltage or power factor at the POI.

This section briefly presents the DFIG WT and reactive power control in wind parks. Readers should refer to [14] for more details.

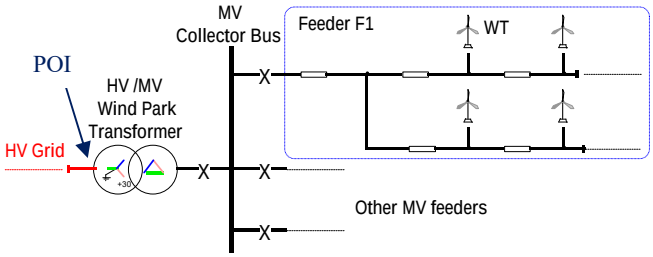

Fig. 1. Simplified single-line diagram of a typical wind park.

A. Reactive Power Control in Wind Farms

The WP reactive power control is based on the secondary voltage control concept [15]. At primary level, WT controller (WTC) monitors and controls its own positive sequence terminal voltage (V_{dfig}) with a proportional voltage regulator. At secondary level, WPC monitors the reactive power at POI (Q_{POI}) and controls it by modifying the WTC reference voltage values ($V'_{dfig} = 1 + \Delta V'_{dfig}$) via a proportional-integral (PI) reactive power regulator, as shown in Fig. 2. Although not shown in Fig. 2, the WPC may also contain voltage control (V-control) and power factor control (PF-control) functions. This paper considers WFC operating under Q-control.

In Fig. 2 and henceforward, all variables are in pu and primed variables are used to indicate the reference values transmitted from controllers.

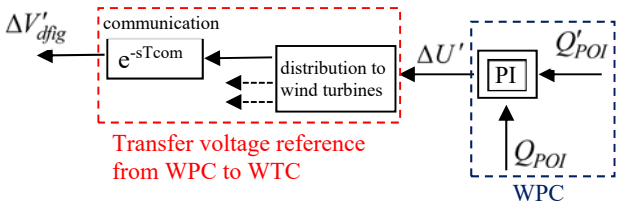

Fig. 2. Reactive power control at the POI (Q-control function).

B. Doubly-Fed Induction Generator Wind Turbines

In WTs with DFIG, the stator of the induction generator (IG) is directly connected to the grid and the wound rotor is connected to the grid through an ac-dc-ac converter system as shown in Fig. 3. The ac-dc-ac converter system consists of two voltage source converters: rotor side converter (RSC) and grid side converter (GSC). A line inductor and shunt harmonic ac filters are used at the GSC to improve power quality (not shown in Fig. 3). A crowbar is used to protect the RSC against overcurrent and the dc capacitor against overvoltage. During crowbar ignition, the RSC is blocked and the IG consumes reactive power. To avoid the crowbar ignition during faults, the dc resistive chopper is used to limit the dc voltage.

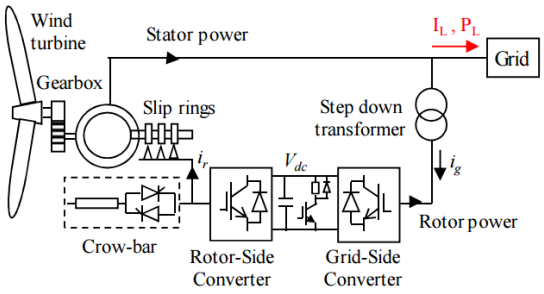

Fig. 3. Schematic diagram of DFIG WT.

C. Doubly-Fed Induction Generator Control and Protection

The simplified diagram of DFIG control and protection system is shown in Fig. 4. The sampled signals are converted to per unit and filtered at "Measurements & Filters" block. The input measuring filters are of low-pass (LP) type. The "Compute Variables" block computes the variables used by the DFIG control and protection system. The "Protection System" block contains cut-in and cut-off speed relays, low voltage and overvoltage relays, GSC and RSC overcurrent protections, dc resistive chopper control and crowbar protection. The "Pitch Control" block limits the mechanical power extracted from wind by increasing the pitch angle when the wind speed is above its rated value.

DFIG converters are controlled using vector control techniques. The RSC operates in the stator flux reference frame and the GSC operates in the stator voltage reference frame. Both RSC and GSC are controlled by a two-level controller. The slow outer control calculates the reference dq-frame currents and the fast inner control allows controlling the converter ac voltage reference.

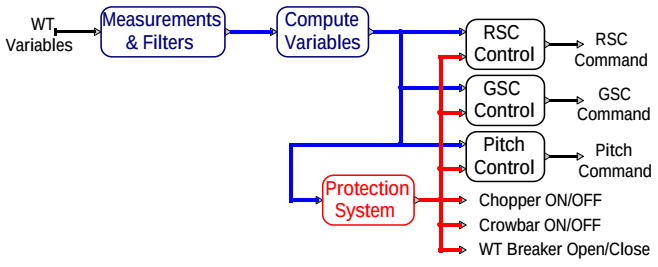

Fig. 4. Simplified diagram of DFIG WT control and protection system.

1) Rotor Side Converter Control

The q- and d-axis currents of the RSC are used to control the active power output and terminal voltage of the DFIG, respectively. The outer loop equations of the RSC are

$$i'_{dr} = (K_v)\left(1 + \Delta V'_{dfig} - V_{dfig}\right) + \left(V_{dfig} / X_m\right)$$
$$i'_{qr} = \left(K_{PP} + K_{IP}/s\right)\left(P'_{dfig} - P_{dfig}\right) \quad (1)$$

where the subscript r stands for rotor, K_v is the voltage regulator gain, K_{PP} and K_{IP} are the power regulator PI parameters. The reference values V'_{dfig} and P'_{dfig} are given by the WPC and the MPPT control, respectively. $\left(V_{dfig}/X_m\right)$ is the compensating term for approximating the reactive current absorbed by the IG and X_m is the IG magnetizing reactance.

During normal operation, the RSC controller gives the priority to the active current, i.e.

$$i'_{dr} < I_{dr}^{\lim} \quad , \; I_{dr}^{\lim} = 1 \; pu$$
$$i'_{qr} < I_{qr}^{\lim} = \sqrt{\left(I_r^{\lim}\right)^2 - \left(i'_{dr}\right)^2} \quad , \; I_r^{\lim} = 1.1 \; pu \quad (2)$$

where $I_{dr}^{\lim}$, $I_{qr}^{\lim}$ and $I_r^{\lim}$ are the limits for d-axis, q-axis and total RSC currents, respectively.

The RSC inner (current) control equations are

$$v_{dr} = \left(K_{Pr} + K_{Ir}/s\right)\left(i'_{dr} - i_{dr}\right) + FF_{dr}$$
$$v_{qr} = \left(K_{Pr} + K_{Ir}/s\right)\left(i'_{qr} - i_{qr}\right) + FF_{qr} \quad (3)$$

where v_{dr} and v_{qr} are the RSC terminal voltages, K_{Pr} and K_{Ir} are the PI control parameters, FF_{dr} and FF_{qr} are the RSC feedforward compensating terms. K_{Pr} and K_{Ir} are determined using IG parameters and the desired RSC rise time ($t_{rise-RSC}$). Readers should refer to [14] for the calculation of K_{Pr} and K_{Ir}, and the expressions for FF_{dr} and FF_{qr}.

2) Grid Side Converter Control

The GSC maintains the dc bus voltage V_{dc} at its nominal value and operates at unity power factor during normal operation. The outer loop equations of the GSC are

$$i'_{dg} = \left(K_{Pdc} + K_{Idc}/s\right)\left(V'_{dc} - V_{dc}\right)$$
$$i'_{qg} = 0 \quad (4)$$

where the subscript g indicates grid, K_{Pdc} and K_{Idc} are the dc voltage controller PI parameters.

The GSC inner (current) control equations are

$$v_{dg} = \left(K_{Pg} + K_{Ig}/s\right)\left(i'_{dg} - i_{dg}\right) + FF_{dg}$$
$$v_{qg} = \left(K_{Pg} + K_{Ig}/s\right)\left(i'_{qg} - i_{qg}\right) + FF_{qg} \quad (5)$$

where v_{dg} and v_{qg} are the GSC terminal voltages, K_{Pg} and K_{Ig} are the PI control parameters, FF_{dg} and FF_{qg} are the GSC feedforward compensating terms. K_{Pg} and K_{Ig} are determined using the equivalent grid impedance seen from the GSC terminals and the desired GSC rise time ($t_{rise-GSC}$). More details are available in [14] for the calculation of K_{Pg} and K_{Ig}, and the expressions for FF_{dg} and FF_{qg}.

D. Fault-Ride-Through (FRT) Function

The WTs are equipped with an FRT function to fulfill the grid code requirement regarding voltage support shown in Fig. 5. The FRT function is activated when the voltage deviation $\left|1 - V_{dfig}\right|$ exceeds the pre-defined value V_{FRT-ON} and deactivated when the voltage deviation reduces below the pre-defined value $V_{FRT-OFF}$ after a pre-specified release time t_{FRT}. When the FRT function is active, the DFIG injects reactive current proportionally to voltage deviation from 1pu (see Fig. 5).

During FRT operation the RSC controller gives the priority to the reactive current by reversing the d- and q-axis current limits given in (2). The GSC also injects reactive currents during faults when the RSC reactive current contribution is not sufficient to satisfy the grid code requirement due to the reactive current absorbed by the IG.

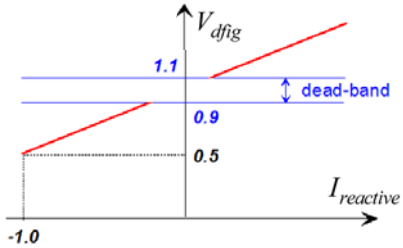

Fig. 5. Wind turbine reactive output current during voltage disturbances [13].

III. System Under Study

The studied network shown in Fig. 6, is inspired from an actual system. The WP contains 400 DFIG WTs of 1.5 MW. It is connected to two large systems, System-1 and System-2, through the transmission lines Line-1 and 2. Line-1 is series compensated by two identical capacitor banks located at its ends, that provide a total of 50% compensation level. The line also contains 230 Mvar shunt reactors at both ends. When Line-2 is disconnected, it leaves the WP radially connected to the series capacitor compensated line Line-1. In that case, the electrical system seen from the DFIG terminals has a series resonance at 30.7 Hz as shown in Fig. 7.

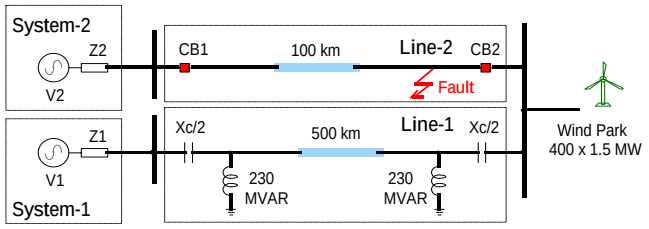

Fig. 6. System under study.

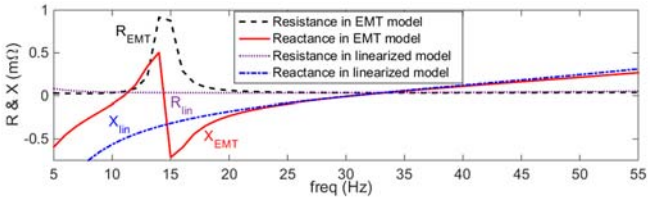

Fig. 7. Impedance seen from DFIG terminals when Line-2 is disconnected.

In EMT simulations, the generic DFIG based WP model presented in [14] is used for 400 WTs. The DFIG converters are represented with average value models (AVMs). Lines-1 and -2 are represented with distributed constant parameter models. A metallic fault is applied at the WP end of Line-2 and cleared with the operation of Line-2 circuit breakers CB1 and CB2. The operating times of CB1 and CB2 are 80 and 60 ms, respectively. The simulation time step is 50 µs in all EMT simulations.

As shown in Fig. 8, the EMT model of the WP consists of an aggregated DFIG WT, an aggregated DFIG transformer, a PI circuit that represents the equivalent MV collector grid, and the HV/MV WP transformer. The aggregated DFIG WT model per unit (pu) parameters are the same with the single DFIG WT pu parameters in aggregation when

$$S_{agg} = N\, S_{WT} \tag{6}$$

where S_{WT} is the single WT base power, N is the number of WTs in aggregation and S_{agg} is the base power for the aggregated WT.

The parameters for the equivalent MV collector grid are calculated on basis of active and reactive power loss in the feeder for the rated current flow from each of the WTs [16].

The AVM replicates the average response of switching devices, converters and controls through simplified functions and controlled sources [17]. AVMs have been successfully developed for wind generation technologies [18], [19]. The AVM of the DFIG is obtained by representing DFIG converters with controlled voltage sources on the ac side and controlled current sources on the dc side, as shown in Fig. 9 [20].

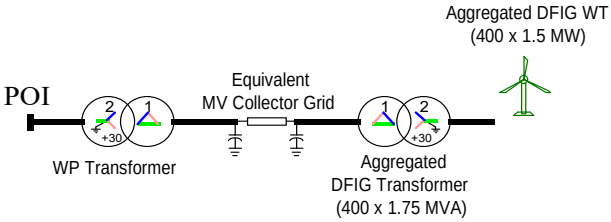

Fig. 8. Wind park EMT model.

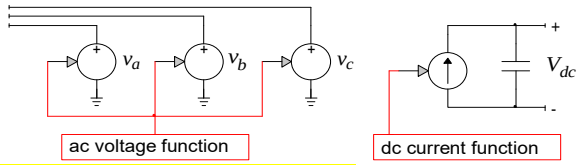

Fig. 9. AVM diagram of the DFIG converters.

The diagram of the radially compensated WP model used in eigenvalue analysis, is shown in Fig. 10. The series capacitor compensated transmission line, the wind farm transformer, the equivalent collector grid and the aggregated DFIG transformers are represented with a single RLC branch. All shunt branches (except the DFIG aggregated harmonic filters) are disregarded. This simplification results a difference in the impedance seen from the DFIG terminals. However, this difference is not significant around series resonant frequency, as shown in Fig. 11. The series resonant frequency is around 30.7 Hz in EMT model and around 30.6 Hz in simplified linearized model. $R_{EMT} \approx 0.0336\ \Omega$ at 30.7 Hz and $R_{lin} \approx 0.0339\ \Omega$ at 30.6 Hz.

The state-space representation of the IG, electrical network (the RLC branch in Fig. 10), choke filter, DC bus and torsional dynamics can be found in [21]. The control system equations are given in (1), (3), (4) and (5). The linearized model of the electrical system is in dq reference frame. It disregards the DFIG input measuring filters and the PLL dynamics. Due to space limitation, the linearization procedure is not given here.

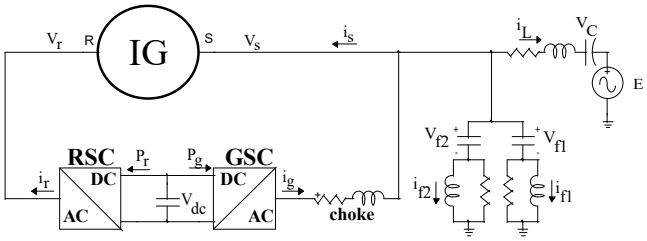

Fig. 10. Radially compensated wind park model used in eigenvalue analysis.

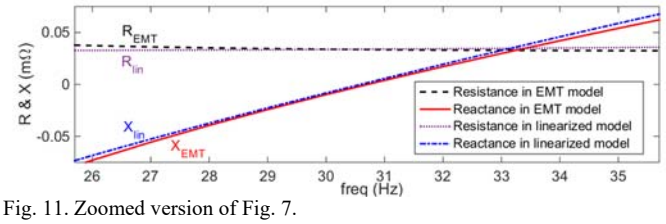

Fig. 11. Zoomed version of Fig. 7.

IV. Impact of Wind Park Operating Conditions

Using the Line-2 outage scenario for different wind speeds, the impact of WP reactive power and WT outages on SSCI mode damping is illustrated in Fig. 12 and Fig. 13, respectively. The impact of WP reactive power generation on SSCI mode damping is not significant. However, SSCI mode damping reduces with wind speed and the potential SSCI problem is expected to be more severe at the slowest permissible wind speed (V = 0.6 pu) when there are 150 to 200 WTs in service. It should be noted that, the collector grid equivalent impedance is kept constant in WT outage scenarios. In reality, large numbers of WT outages result from collector grid feeder outages. Increase in the collector equivalent impedance (both resistance and inductance) due to feeder outages, will result into larger SSCI mode damping values as compared to the ones presented in Fig. 13.

Several EMT simulations are performed to validate the eigenvalue analysis results. However, only the simulation scenarios in Table I are presented in Fig. 14 - Fig. 16 due to space limitations. Although a large disturbance is simulated, the EMT simulation results correlate with the eigenvalue analysis results. In other words, the impact of wind speed, WP reactive power and WT outages on SSCI mode is similar in both studies. However, the SSCI mode dampings in EMT simulations are much lower compared to the ones obtained in eigenvalue analysis. All the scenarios presented in Table I have positive SSCI mode damping. However, the SSCI mode is unstable in scenarios S4, S5, S8 and S9 as shown in Fig. 14 and Fig. 16. As demonstrated in Section VII, the DFIG input measuring filters have significant impact on SSCI and their omission in the linearized system model mainly causes this significant difference.

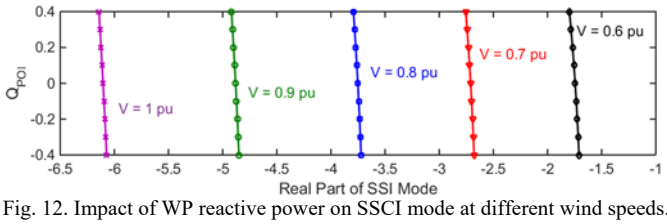

Fig. 12. Impact of WP reactive power on SSCI mode at different wind speeds.

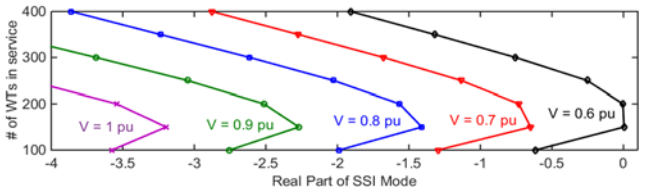

Fig. 13. Impact of WT outages on SSCI mode at different wind speeds.

Table I: EMT simulations (impact of WP operating conditions)

	S1	S2	S3	S4	S5	S6	S7	S8	S9
V (pu)	1	0.9	0.8	0.7	0.6	0.8	0.8	0.8	0.8
Q_{POI} (pu)	0	0	0	0	0	0.2	-0.2	0	0
# of WTs	400	400	400	400	400	400	400	300	200

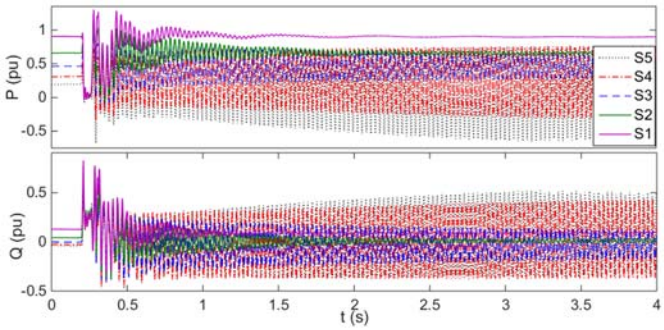

Fig. 14. Impact of wind speed on SSCI mode damping.

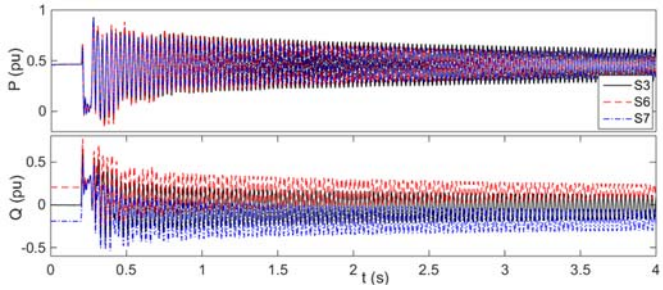

Fig. 15. Impact of WP reactive power on SSCI mode damping.

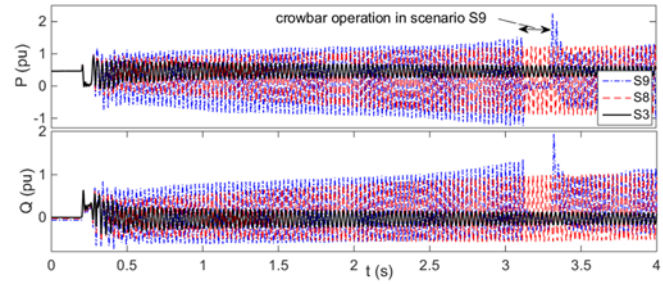

Fig. 16. Impact of WT outages on SSCI mode damping.

V. Impact of DFIG Control System Parameters

The impacts on SSCI mode damping of the inner control loop parameters in the RSC and GSC are illustrated in Fig. 17 and Fig. 18, respectively. In these cases, Line-2 remains disconnected and wind speed variation is again applied. The impact of GSC rise time on SSCI mode damping is not significant. On the other hand, increasing RSC rise time provides significant improvement in SSCI mode damping.

Large RSC rise time usage will cause sluggish DFIG transient response to faults. However, it is possible to compensate the sluggish inner current loop response by increasing the voltage regulator gain. As shown in Fig. 19, the increase in voltage regulator gain also slightly improves SSCI mode damping. The slow outer control loops of RSC and GSC do not have significant impact on SSCI [1],[2].

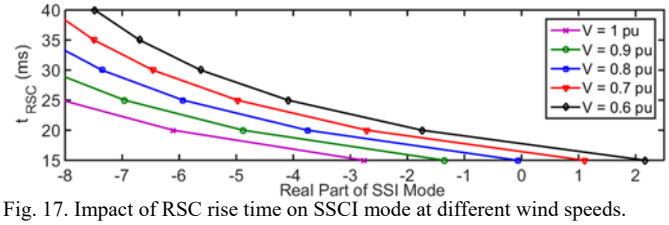

Fig. 17. Impact of RSC rise time on SSCI mode at different wind speeds.

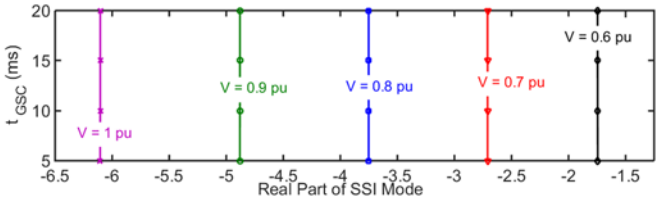

Fig. 18. Impact of GSC rise time on SSCI mode at different wind speeds.

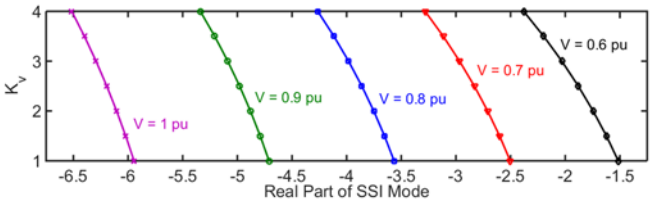

Fig. 19. Impact of voltage regulator gain on SSCI mode at different wind speeds.

The EMT simulation results for the scenarios in Table II are presented in Fig. 20 and Fig. 21. In all scenarios the WP operating conditions are the same as in scenario S3 of Table I. The parameters in Scenario S11 are the original parameters in [14]. The EMT simulation results correlate with the eigenvalue analysis results. The lower SSCI mode damping in EMT simulations when compared to eigenvalue analysis, is once again due to absence of DFIG input measuring filters in the linearized system model.

Table II: EMT simulations (impact of WT control system parameters)

	S10	S11	S12	S13	S14
$t_{rise-RSC}$ (ms)	15	20	25	20	20
K_v	2	2	2	2.5	3

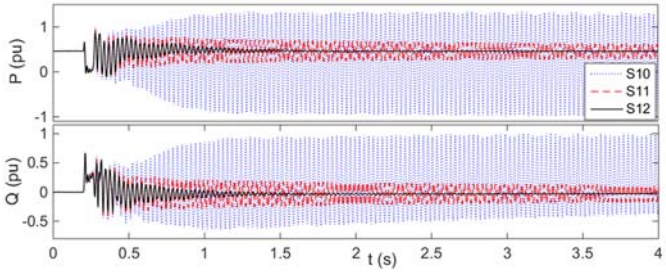

Fig. 20. Impact of RSC rise time on SSCI mode damping.

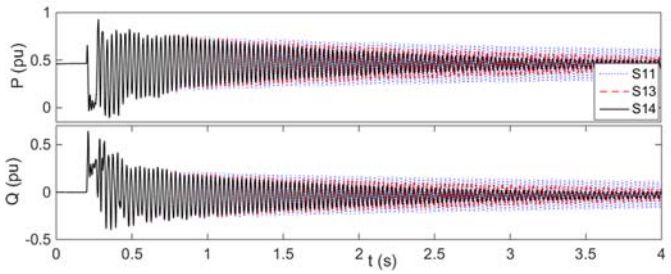

Fig. 21. Impact of voltage regulator gain on SSCI mode damping.

VI. Proposed Frequency Scan Analysis Approach

The turbine side impedance scan at the low voltage (LV) bus for the aggregated WT model is obtained in this paper using a sinusoidal current excitation (see Fig. 22). It is also possible to use voltage excitation. It is presented in Fig. 23. The zoomed version of Fig. 23 is shown in Fig. 24. In the simulation model, DFIG converters are represented with their AVMs. The simulation time step is 50 µs. More details on this approach are available in [22].

The focus in turbine side impedance scans is identifying reactance crossover and negative resistance in the subsynchronous frequency range. The criteria or conditions that pose higher risk of SSCI [23], [24] are:

1. any reactance crossovers on the turbine side that coincide with resonant conditions on the system side,
2. any resonant condition on the system side if the turbine resistance at that subsynchronous frequency is negative.

According to the second criteria, there is a high risk of SSCI for all simulation scenarios presented in Fig. 14 (S1 - S5 in Table I) as the electrical system has a resonant condition at 30.7 Hz and the turbine resistance is negative for the subsynchronous frequency range greater than 15 Hz as shown in Fig. 24.

The second criteria considers the resonant frequencies identified by the system side frequency scan alone, i.e. disregards the contribution of the WP. In reality, the WP contribution may result into totally different resonant conditions. A more accurate prediction can be obtained by adding the turbine side and grid side impedances (combined scan analysis shown in Fig. 25). Any reactance crossover in combined scan with negative total resistance, indicates potential SSCI.

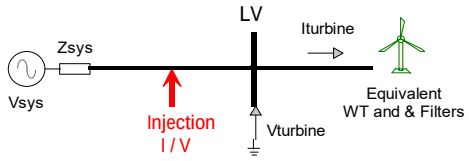

Fig. 22. Voltage and/or current injection-based turbine side scan.

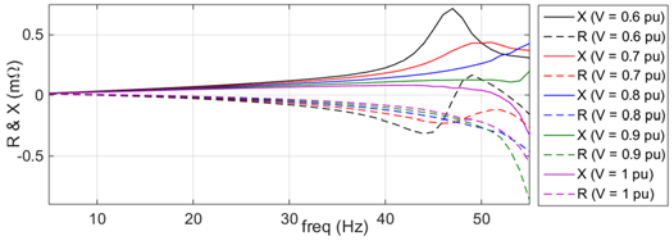

Fig. 23. Turbine side scan for various wind speeds (Q_{POI} = 0, # of WTs = 400).

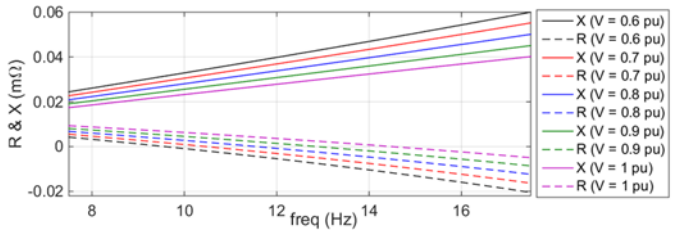

Fig. 24. Zoomed version of Fig. 23.

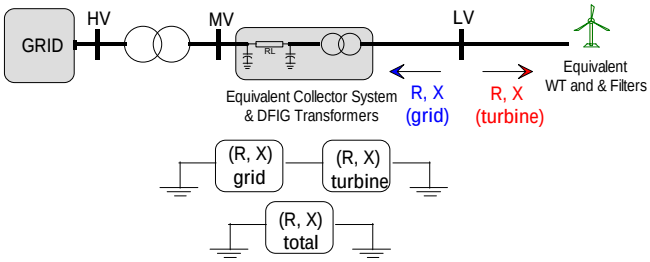

Fig. 25. Illustration of combined scan analysis.

The total reactance and resistance (X_{total} and R_{total}) are shown in Fig. 26 for scenario S1. The zoomed version of Fig. 26 is given in Fig. 27. The resonant frequency of the system is 26.7 Hz and the total resistance of the system is positive at this frequency. Unlike the original criteria, the proposed criteria does not indicate any SSCI problem. It is observed that the SSCI mode frequency is around 26.7 Hz in both eigenvalue analysis and EMT simulations.

The total reactance and resistance are shown in Fig. 28 for scenarios S2 - S5. The resonant frequencies in scenarios S2 to S5 are 26.1 Hz, 25.6 Hz, 25.2 Hz and 24.8 Hz, respectively. In Fig. 28, R_{S2}, R_{S3}, R_{S4}, and R_{S5} are the total resistances at resonant frequencies in S2, S3, S4 and S5, respectively. The total resistance at resonant frequency increases with the increase in wind speed ($R_{S2} > R_{S3} > R_{S4} > R_{S5}$). R_{S4}, and R_{S5} are negative, which means that the combined scan analysis indicates SSCI problem in scenarios S4 and S5. The EMT simulation results presented in Fig. 14 confirm the accuracy of the combined scan analysis.

R_{S3} is positive, but it is very close to zero as shown in Fig. 28. Although not apparent in Fig. 14 and Fig. 15, the considered WP also suffers from SSCI problem in scenario S3. The subsynchronous frequency oscillations do not damp completely as shown in Fig. 29.

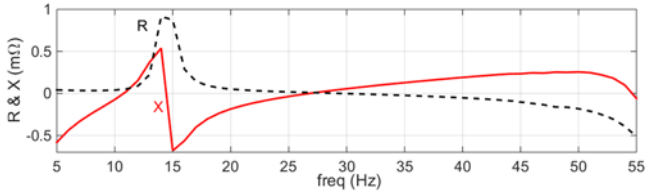

Fig. 26. Combined scan for Scenario S1.

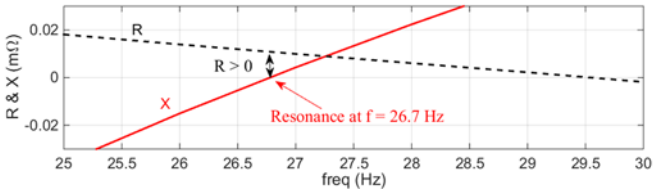

Fig. 27. Zoomed version of Fig. 26.

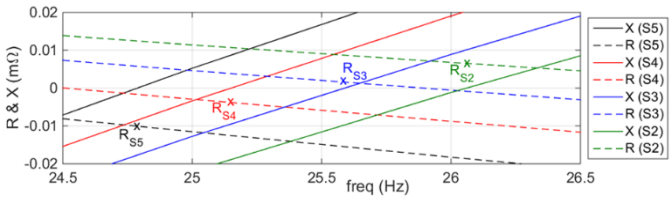

Fig. 28. Combined scan for Scenarios S2-S5.

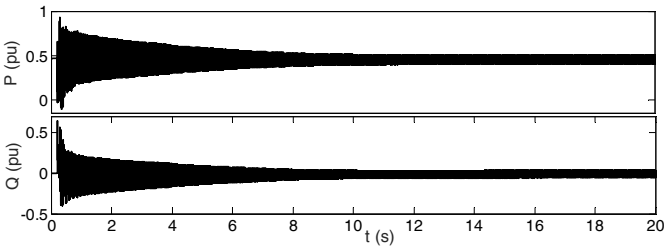

Fig. 29. Active and reactive powers in scenario S3.

VII. Impact of DFIG Input Measuring Filters

The considered DFIG [14] uses 4th order Bessel type LP input measuring filters. The cut-off frequencies (fc) of these filters are 4.5 kHz and 2.25 kHz for GSC and RSC, respectively. The sampling frequencies (fs) are 22.5 kHz and 11.25 kHz at GSC and RSC, respectively. These filters introduce a phase shift in the measured signals. This phase shift depends on the filter type, order and cut-off frequency.

The impact of these filters on turbine side impedance scan is presented in Fig. 30 and Fig. 31 for the scenarios given in Table III. In all scenarios, the WP operating conditions are the same as in the scenario S3 in Table I. It should be noted that the scenario S16 is the same as S3.

Table III: EMT simulations (impact of DFIG input measuring filters)

	S15	**S16 (S3)**	**S17**	**S18**	**S19**
fc	2.5 x fs	5 x fs	10 x fs	5 x fs	5 x fs
order	4	4	4	2	6

The phase-shift introduced by the input measuring filter increases with the increase in its order and decrease in its cut-off frequency. As shown in Fig. 30 and Fig. 31, the turbine side resistance decreases with the increase in phase-shift introduced by the input measuring filter. Using high order filter and/or low cut-off frequency makes the system vulnerable to SSCI as shown in Fig. 32. In Fig. 32, R_{S15}, R_{S16}, R_{S17}, R_{S18} and R_{S19} are the total resistances at resonant frequencies in S15, S16, S17, S18 and S19, respectively. $R_{S17} < 0$ and $R_{S19} \approx 0$, which indicates instability. SSCI mode damping is highest in S15 for the scenarios in Table III since S15 has the largest resistance at the resonant frequency. The EMT simulation results shown in Fig. 33 confirm the accuracy of the combined scan analysis results presented in Fig. 32.

It should be noted that, as the phase shift introduced by the DFIG input measuring filters decreases, discrepancies between the eigenvalue analysis and EMT simulation results become less noticeable.

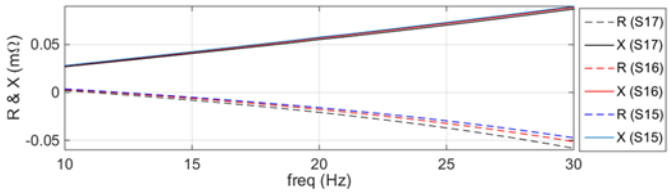

Fig. 30. Turbine side scan for scenarios S15 - S17.

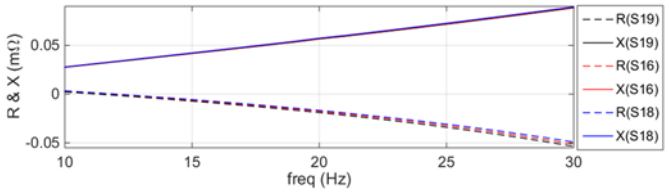

Fig. 31. Turbine side scan for scenarios S16, S18, S19.

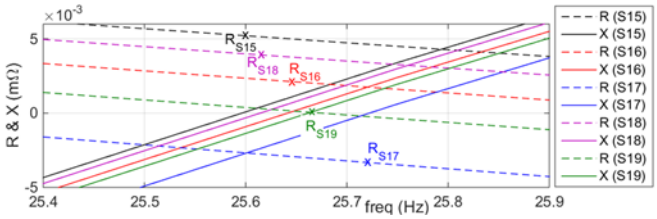

Fig. 32. Combined scan for scenarios S15 - S19.

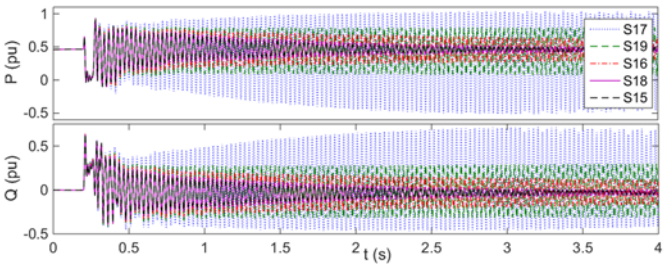

Fig. 33. Impact of DFIG input measuring filters on SSCI mode damping.

VIII. Guidelines for Safe Operation

The potential SSCI problem is expected to be more severe at slow wind speeds and for extreme WT outage scenarios as demonstrated in Section IV. Hence SSCI studies for safe operation should consider such extreme WP operating conditions.

As demonstrated in Section V, the RSC rise time has significant impact on SSCI mode damping. Therefore, this paper proposes increasing the RSC rise time to achieve the desired SSCI mode damping. The sluggish inner current loop response can be compensated by using a larger voltage regulator gain to avoid any deterioration in DFIG transient performance.

The deterioration in DFIG transient performance due to large RSC rise time usage and its correction by a larger voltage regulator gain is demonstrated by simulating a three-phase high impedance fault in the simple infinite bus system shown in Fig. 34. As small impedance faults (metallic) cause severe voltage sags at the DFIG terminal, the GSC contributes to the DFIG reactive currents and the deterioration in the DFIG transient performance due to large RSC rise time usage becomes less noticeable. The simulation scenarios are given in Table IV.

The reactive (d-axis) currents of RSC and DFIG terminal voltages presented in Fig. 35, demonstrate the deterioration in DFIG transient performance due to large RSC rise time usage. However, this can be corrected with a small increase in voltage regulator gain as shown in Fig. 36. An increase in the voltage regulator gain also slightly improves SSCI mode damping.

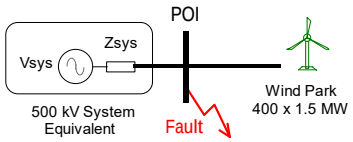

Fig. 34. Simple infinite bus system for testing DFIG transient performance.

Table IV: EMT simulations (DFIG transient performance)

	S20	S21	S22	S23	S24
$t_{rise-RSC}$ (ms)	20	30	40	30	40
K_v	2	2	2	2.2	2.4

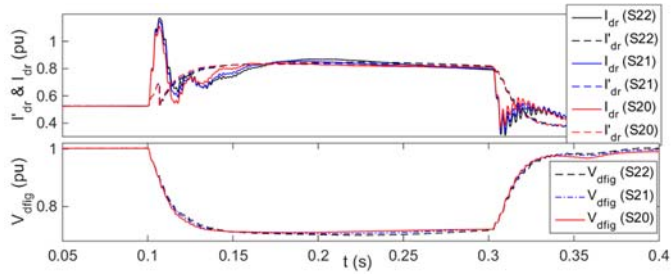

Fig. 35. DFIG transient performance in Scenarios S20 - S22.

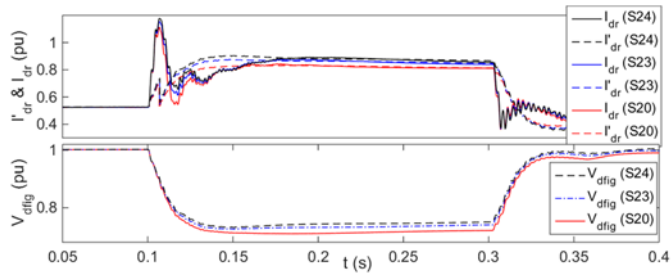

Fig. 36. DFIG transient performance in Scenarios S20, 23, 24.

As demonstrated in Section VII, the SSCI mode damping decreases with the increase in phase shift introduced by the DFIG input measuring filters. Hence, high order filter usage should be avoided. Also a possible improvement is to increase the filter cut-off frequency. It should be noted, that the DFIG control sampling frequency introduces a strict limit on the highest possible filter cut-off frequency.

The guidelines for the safe operation is as follows:

- avoid (if possible) using high order and low cut-off frequency DFIG input measuring filters;
- consider extreme WP operating conditions, such as the permissible slowest wind speed, and extreme WT outages to identify the scenario with lowest SSCI mode damping;
- increase the RSC rise time (if necessary) to improve the desired SSCI mode damping;
- check the DFIG transient performance with the increased RSC rise time and increase the voltage regulator gain (if necessary) to achieve the acceptable DFIG transient performance.

Based on the above guidelines, the modifications in Table V are proposed in DFIG control system parameters. The EMT simulations presented in Fig. 37 consider the WP operating conditions with the lowest SSCI mode damping in scenario S25 (V = 0.6 pu, Q_{POI} = 0 pu, 200 WTs) in addition to scenario S5 (lowest SSCI mode damping for no WT outage). The results presented in Fig. 37 demonstrate that, the proposed DFIG parameters provide the desired SSCI damping and the acceptable transient response to the faults.

Table V: Proposed in DFIG control system parameters

	$t_{rise-RSC}$	K_v	filter order	cut-off frequency (fc)
Original	20 ms	2	4	5 × fs
Proposed	30 ms	2.2	2	2.5 × fs

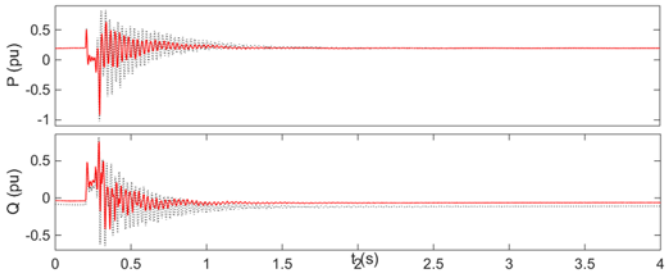

Fig. 37. Performance with proposed DFIG parameters, red for S5 and black-dashed for S25.

IX. Conclusion

This paper presented a methodology for modifying the DFIG control system parameters to ensure safe operation in a series compensated system while maintaining acceptable DFIG transient response to faults. A severe SSCI problem in a practical DFIG based series compensated WP is mitigated by applying the presented methodology. The desired SSCI mode damping is achieved by increasing the RSC rise time. The resulting sluggish inner current loop response is compensated by increasing the voltage regulator gain.

This paper also demonstrated that the DIFG input measuring filters have significant impact on SSCI. The SSCI mode damping decreases with the increase in phase-shift introduced by the input measuring filter. Therefore, high order filter usage should be avoided. The SSCI mode damping can be improved further by increasing the filter cut-off frequency. On the other hand, the DFIG control sampling frequency introduces a strict limit for the highest possible filter cut-off frequency.

The linearized model of the electrical system is in dq reference frame and it disregards the DFIG input measuring filters. This causes large discrepancies between eigenvalue analysis and EMT simulation results, especially when DFIG input measuring filter introduces a large phase-shift.

This paper also proposed a new frequency scan analysis approach for accurate prediction of SSCI problems. The proposed approach considers the contribution of the WP to the resonance condition. The accuracy of the proposed approach has been confirmed with several EMT simulations for various WP operating conditions and DFIG control system parameters.

REFERENCES

[1] L. Fan, C. Zhu, Z. Miao and M. Hu, "Modal Analysis of a DFIG-Based Wind Farm Interfaced With a Series Compensated Network," *IEEE Trans. on Energy Conversion*, vol. 26, no. 4, pp. 1010-1020, Dec. 2011.

[2] A. Ostadi, A. Yazdani, and R. Varma, "Modeling and stability analysis of a DFIG-based wind-power generator interfaced with a series-compensated line," *IEEE Trans. on Power Delivery*, vol. 24, no. 3, pp. 1504-1514, July 2009.

[3] L. C. Gross, "Sub-synchronous grid conditions: New event, new problem, and new solutions," in *Proc. 37th Annual Western Protective Relay Conf.*, Spokane, WA, USA, Oct. 2010, pp. 1–19.

[4] G. D. Irwin, A. K. Jindal and A. L. Isaacs, "Sub-synchronous control interactions between Type 3 wind turbines and series compensated AC transmission systems," in *Proc. IEEE PES Gen. Meet.*, Detroit, MI, USA, Jul. 2011, pp. 1–6.

[5] NERC. (2011, Jul. 26). "Lesson learned—Sub-synchronous interaction between series-compensated transmission lines and generation," Online Rep. Lesson Learned#: 20110705 [Online]. Available: http://www.nerc.com/files/LL_45_Sub-Synchronous_Interaction.pdf.

[6] A. E. Leon and J. A. Solsona, "Sub-Synchronous Interaction Damping Control for DFIG Wind Turbines," *IEEE Trans. on Power Systems*, vol. 30, no. 1, pp. 419-428, Jan. 2015.

[7] R. K. Varma, S. Auddy and Y. Semsedini, "Mitigation of Subsynchronous Resonance in a Series-Compensated Wind Farm Using FACTS Controllers," *IEEE Trans. on Power Delivery*, vol. 23, no. 3, pp. 1645-1654, July 2008.

[8] U. Karaagac, S. O. Faried, J. Mahseredjian and A. A. Edris, "Coordinated Control of Wind Energy Conversion Systems for Mitigating Subsynchronous Interaction in DFIG-Based Wind Farms," *IEEE Trans. on Smart Grid*, vol. 5, no. 5, pp. 2440-2449, Sep. 2014.

[9] H. A. Mohammadpour and E. Santi, "SSR Damping Controller Design and Optimal Placement in Rotor-Side and Grid-Side Converters of Series-Compensated DFIG-Based Wind Farm," *IEEE Trans. on Sustainable Energy*, vol. 6, no. 2, pp. 388-399, April 2015.

[10] C. Zhu, L. Fan and M. Hu, "Control and analysis of DFIG-based wind turbines in a series compensated network for SSR damping," in *Proc. IEEE PES Gen. Meet.*, Minneapolis, MN, 2010, pp. 1-6.

[11] L. Fan and Z. Miao, "Mitigating SSR Using DFIG-Based Wind Generation," *IEEE Trans. on Sustainable Energy*, vol. 3, no. 3, pp. 349-358, July 2012.

[12] P. H. Huang, M. S. El Moursi, W. Xiao and J. L. Kirtley, "Subsynchronous Resonance Mitigation for Series-Compensated DFIG-Based Wind Farm by Using Two-Degree-of-Freedom Control Strategy," *IEEE Trans. on Power Systems*, vol. 30, no. 3, pp. 1442-1454, May 2015.

[13] "Grid code - high and extra high voltage," E.ON Netz GmbH, Bayreuth, Germany, April 2006.

[14] U. Karaagac, H. Saad, J. Peralta and J. Mahseredjian, "Doubly-fed induction generator based wind park models in EMTP-RV", April 2015, Polytechnique Montréal. Available at: www.??????????

[15] J. M. Garcia, "Voltage control in wind power plants with doubly fed generators," Ph.D. dissertation, Aalborg Univ., Denmark, Sep. 2010.

[16] E. Muljadi, C.P. Butterfield, a Ellis, J. Mechenbier, J. Hochheimer, R. Young, N. Miller, R. Delmerico, R. Zavadil, and J.C. Smith, "Equivalencing the collector system of a large wind power plant," in *Proc IEEE PES Gen. Meet.*, Montreal, CA, June 18-22, 2006.

[17] S. R. Sanders, J. M. Noworolski, X. Z. Liu, and G. C. Verghese, "Generalized averaging method for power conversion circuits," *IEEE Trans. on Power Electronics*, vol. 6, no. 2, pp. 251–259, Apr. 1991.

[18] J. Morren, S. W. H. de Haan, P. Bauer, J. Pierik, and J. Bozelie, "Comparison of complete and reduced models of a wind turbine with Doubly-fed Induction Generator," in *Proc. 10th Eur. Conf. Power Electron. Appl.*, Toulouse, France, Sep. 2003, pp. 1–10D.

[19] J. G. Slootweg, H. Polinder, and W. L. Kling, "Representing wind turbine electrical generating systems in fundamental frequency simulations," *IEEE Trans. on Energy Conv.*, vol. 18, no. 4, pp. 516-524, Dec. 2003.

[20] J. Peralta, H. Saad, U. Karaagac, J. Mahseredjian, S. Dennetière and X. Legrand, "Dynamic Modeling of MMC-based MTDC Systems for The Integration of Offshore Wind Generation," *CIGRE Canada conference on Power Systems*, September 2012, Montreal.

[21] L. Fan and Z. Miao, Modeling and Analysis of Doubly Fed Induction Generator Wind Energy Systems, Academic Press, April 2015.

[22] U. Karaagac, H. Gras and J. Mahseredjian, "Automated Subsynchronous Frequency Range Turbine Side Scanning in EMTP-RV", April 2015, Polytechnique Montréal. Available at: www.??????????.

[23] B. Badrzadeh, M. Sahni, D. Muthumuni, Y. Zhou and A. Gole, "Sub-Synchronous Interaction in Wind Power Plants – Part I: Study Tools and Techniques," in *Proc IEEE PES Gen. Meet.*, San Diego, CA, July 22-26, 2012.

[24] B. Badrzadeh, M. Sahni, Y. Zhou, D. Muthumuni, and A. Gole, "General Methodology for Analysis of Sub-Synchronous Interaction in Wind Power Plants," *IEEE Trans. On Power Systems*, 2013, vol. 28, no.2, pp. 1858-1869.